Version January 15, 2025
Preprint typeset using LaTeX style openjournal v. 09/06/15

Dwarf galaxies don't just form stars, they have BURSTS of star formation. We're looking at the chemical evidence left behind.

QUANTIFYING BURSTY STAR FORMATION IN DWARF GALAXIES

Yuan-Sen Ting (丁源森)
Department of Astronomy, The Ohio State University, Columbus, OH 43210, USA
Center for Cosmology and AstroParticle Physics (CCAPP), The Ohio State University, Columbus, OH 43210, USA and
Research School of Astronomy & Astrophysics, Australian National University, Cotter Rd., Weston, ACT 2611, Australia

Alexander P. Ji
Department of Astronomy & Astrophysics, University of Chicago, 5640 S Ellis Avenue, Chicago, IL 60637, USA and
Kavli Institute for Cosmological Physics, University of Chicago, Chicago, IL 60637, USA
Version January 15, 2025

SUMMARY

ABSTRACT

Dwarf galaxies are weird. They have episodes where they form lots of stars, and then quiet periods where they don't.

We're using the chemical composition of their stars to figure out the timing of these "bursts" and "quiet" phases.

TL;DR: Star formation in dwarfs is like a flickering candle, not a steady flame, and we can read the history in the stars' chemistry.

Keywords:

1. INTRODUCTION

WHY BOTHER?

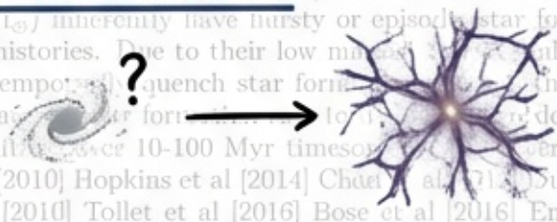

Because understanding how dwarf galaxies form stars is key to understanding the whole universe, especially its early history (like reionization). They're the building blocks!

Star Formation History (SFH)

The Chemical Clue!

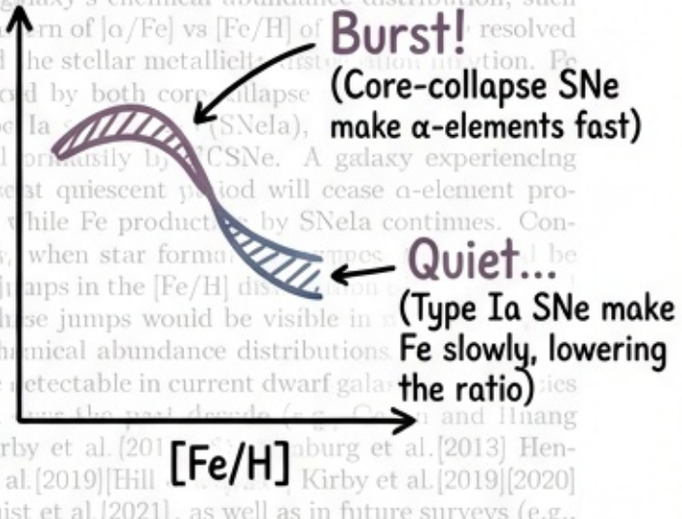

We're hunting for these specific chemical patterns!

So, how do we find these chemical clues?
We build a SIMPLE MODEL!

A Recipe for a "Toy" Dwarf Galaxy

THE INGREDIENTS:

- Bursty Star Formation:
  Stars form in quick episodes.

- Two Element "Factories":
  (1) Fast Factory (CCSNe):
  Makes α-elements (like Mg) INSTANTLY.

  (2) Slow Factory (SNIa):
  Makes Iron (Fe) with a DELAY.

The math for the iron *delay* time.

A HUGE SIMPLIFICATION:
We assume the total amount of gas available is CONSTANT.
It's like a "closed box" that moves with the galaxy.

smooth prescriptions for gas and star formation histories (SFH) (e.g., Cescutti 2005] Kirby et al. 2011a] Pilkington and Gibson 2012] Vincenzo et al. 2015] Recchi and Kroupa 2013] [shimaru et al. 2017] Coté et al [2017] Weinberg et al. 2017] Matroucci 2021] de los Reyes et al. 2023) Johnson et al. 2023] Sandford et al. 2023), with some notable exceptions (e.g., Hirashito et al. 2021] Johnson and Weinberg 2023). Some semi-analytic [illegible] merger trees, allow for [illegible] study the impact on individual metallicity distributions (e.g., Lu et al. 2011] [illegible] (2023) [illegible] bursty star formation (e.g., Jeon et al. 2011] Wheeler et al. 2018] Applebaum et al. 2021). but they are still relatively limited in mass and time resolution for studying the early chemical evolution of dwarf galaxies and [illegible]

To address this gap, we propose that bursty star formation enforces [illegible] that 2]. The model predicts a multimodal chemical pattern (Section 2], which we suggest can be [illegible] as a [illegible] We apply this test to [illegible] perience [illegible] conclude by discussing prospects for future abundance surveys and comparisons to high-redshift observations (Sections 6 and 7].

2. SIMPLE CHEMICAL EVOLUTION MODEL

To understand how bursty star formation can lead to a distinctive discontinuous chemical track, we draw intuition from a simplified setup for the chemical evolution of a dwarf galaxy, which allows us to integrate the chemical track analytically by varying only the star formation history and the underlying mixing gas mass. We will trace the α-elements with the Mg abundance, as it is relatively easy to measure in stars and uncontaminated by SNIa yields (e.g., Kirby et al (2019] Skiiladóttir et al [2019, Weinberg et al (2019). We adopt the standard one-zone, instantaneous mixing approximation, which is likely applicable for dwarf galaxies due to their small sizes (e.g., Kirby et al [2011a, Vincenzo et al [2019, Johnson et al. 2023).

We assume a prompt source of stellar yield from core-collapse supernovae (CCSNe), which produces both Mg and Fe 10 Myr after a starburst:

$$D_{\rm CC}(t) = \delta\left(\left(\frac{t}{\rm Myr}\right) - 10\right), \qquad (1)$$

and a delayed source for Type Ia supernovae (SNeIa), which contribute only to Fe. We assume a power law delay time distribution with index -1.1 and a minimum delay time of 100 Myr (Maoz et al. [illegible]

$$\begin{cases} 0 & \text{for } t < 100\ \text{Myr} \\ \left(\frac{t}{\rm Myr}\right)^{-1.1} & \text{for } t \geq 100\ \text{Myr} \end{cases} \qquad (2)$$

where 0.420 is a normalization constant. We assume the core-collapse supernova IMF-averaged yield for Fe and Mg per supernova to be $y_{\rm CC,Fe} = 0.051$ and $y_{\rm CC,Mg} = 0.192$ with the rate of $r_{\rm CC} = 0.01\ {\rm M}_\odot^{-1}$ core-collapse supernovae per solar mass formed, and the Type Ia supernovae yield of Fe to be $y_{\rm Ia,Fe} = 0.749$ with negligible Mg production, and a supernova rate of $r_{\rm Ia} = 0.189\ {\rm M}_\odot^{-1}$. Time (in $M_\odot$) and rates are adopted from Kirby et al. (2011a).

We then make three simplifying assumptions. First, we assume the yields have no metallicity dependence. This is a reasonable assumption for Mg and Fe in metal-poor dwarf galaxies, where the metallicity dependence of IMF-integrated yields is relatively weak (e.g., Nomoto et al. 2013). Then, the total yield of heavy elements is simply the convolution of the star formation rate, $\dot{M}_*(t)$, [illegible]ed by the yield convolved with the delay time distribution:

$$Y_X(t) = \dot{M}_*(t) * (y_{{\rm CC},X}\, r_{\rm CC} D_{\rm CC}(t) + y_{{\rm Ia},X}\, r_{\rm Ia} D_{\rm Ia}(t)) \qquad (3)$$

where $Y_X(t)$ is the total yield of element X at time t. The total mass of an element X that has ever been produced by a g[illegible]xy at time [illegible] can be expressed as

$$M_X(t) = \int_0 Y_X(t')\, {\rm d}t' \qquad (4)$$

Second, we assume that we can independently specify the star formation rate $\dot{M}_*(t)$ and an effective gas mass $M_{\rm g,eff}(t)$, which includes not just the cold interstellar medium, but also the circumgalactic or intergalactic gas mass that is affected by the stellar yields from this galaxy. The abundance of element X relative to hydrogen at time t can then be calculated as:

$$[X/{\rm H}](t) = \log_{10}\left(\frac{M_X(t)}{\mu_X M_{\rm g,eff}(t)}\right) - \log_{10}\left(\frac{N_X}{N_H}\right)_\odot \qquad (5)$$

where μ_X is the atomic mass of element X, $\log_{10}(N_X/N_H)_\odot$ is the solar abundance ratio of element X to hydrogen (adopted from Asplund et al [2008]. We assume $\mu_X = 24$ for Mg and $\mu_X = 56$ for Fe. We note this assumption is mathematically equivalent to standard [illegible] this galaxy, which co[illegible] lar medium but also [illegible]

Third, and the biggest assumption here, we take the mixing gas mass to be a constant, i.e. $\dot{M}_{\rm g,eff}(t) = 0$. This

Let's see what our "Toy" galaxy predicts!

We'll compare our model to a real galaxy: SCULPTOR dSph (our benchmark)

→ 10 bursts... over a total duration of 2 Gyr

↳ *Our setup: A galaxy with a "hiccup" every ~200 Myr*

→ $M_{g,eff} = 3 \times 10^8 M_{sun}$

↳ *Our constant gas supply (from pg 2)*

→ fiducial chemical evolution model

A more REALISTIC model: Bursts aren't instant, they last ~150 Myr

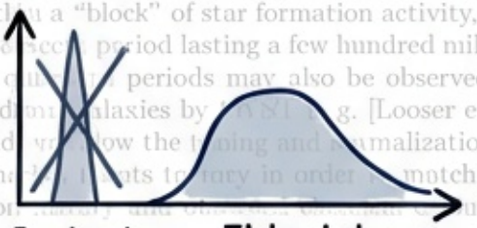

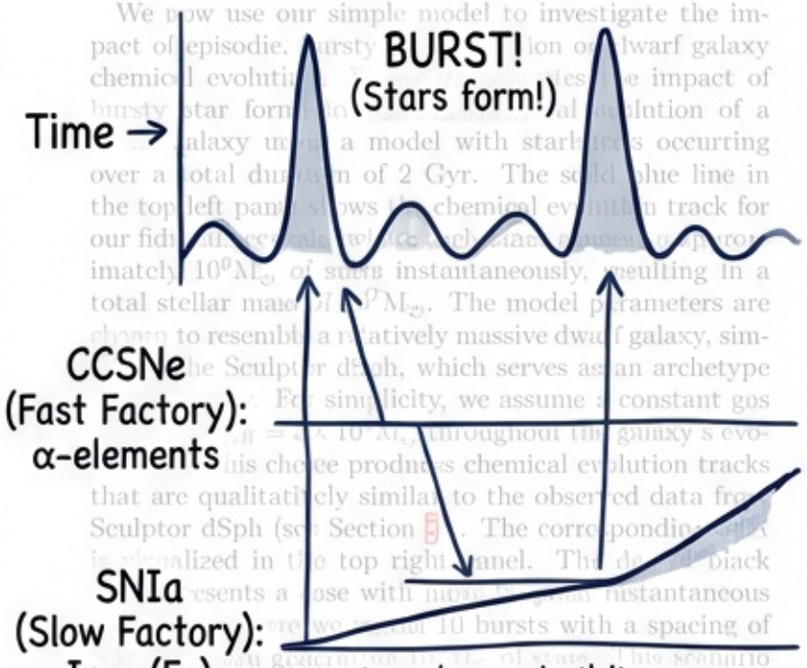

Iron keeps building up during QUIET times...

Fe/H continues to accumulate from Type Ia supernovae during quiescent periods

↓

This creates "gaps" in the chemical plot!

temporal "resolution"... is limited by the minimum delay time for Type Ia supernovae, which is 100 Myr

LIMITATION: Our chemical "clock" can't resolve bursts faster than ~100 Myr (the SNIa delay)

APOGEE

↳ *We'll compare to high-quality data from this survey.*

Here are the results from our "Toy" models!

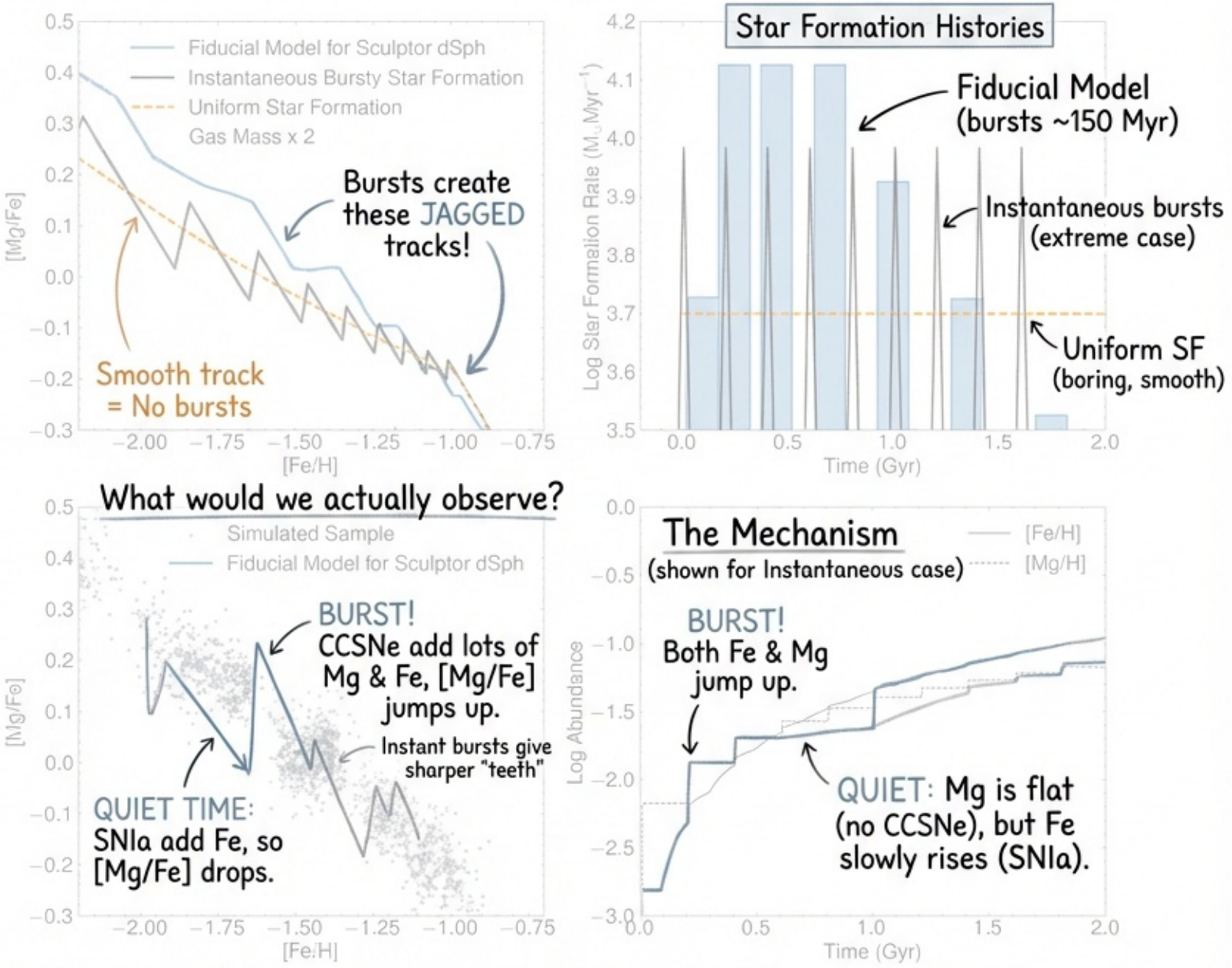

Figure 1. Bursty star formation creates discontinuous chemical tracks in the [Mg/Fe]-[Fe/H] plane. The top left panel shows chemical tracks resulting from various star formation histories: our fiducial model to match the Sculptor dSph observation (solid blue line), star formation with instantaneous bursts every 200 Myr over 2 Gyr (solid black line), continuous star formation (dashed orange line), and a scenario with doubled gas mass (dash-dotted red line). The top right panel displays the corresponding star formation histories. The bottom right panel illustrates the evolution of Fe and Mg abundances in the instantaneous starburst case. It demonstrates that the ISM's [Fe/H] continues to accumulate from instantaneous core-collapse supernovae. This combination creates gaps in the [Mg/Fe]-[Fe/H] plane, where [Fe/H] reflects star formation gaps and [Mg/H] largely follows yields. The bottom left panel presents the simulated abundance data, showing 1000 sampled data points (grey) following the fiducial star formation history, with an assumed measurement error of 0.05 dex, along with their kernel density estimation contours. The distinct clumps found in the [Mg/Fe]-[Fe/H] plane contrast sharply with the continuous star formation case. All modeled star formation rates integrate to a total stellar mass of $3 \times 10^6 M_\odot$, consistent with the Sculptor dSph galaxy, with an effective gas mass of $3 \times 10^6 M_\odot$.

burst case, the chemical evolution track exhibits smooth features, where the slope of the upward spike in [Mg/Fe] is solely determined by the burst. In contrast, our fiducial model with star formation spanning 150 Myr per starburst allows for continuous enrichment of the ISM by Type Ia supernovae during the burst, resulting in more subdued and concave stripes instead of discrete spikes. However, it is important to note that while the instantaneous starburst model might appear to lead to a marginally larger spread in the chemical track, the track represents the chemistry of the gas, not necessarily the observed stars. In the instantaneous case, all stars are created at the base of each spike, rather than being gradually formed as the burst continues over a more prolonged period. As a result, the fiducial model shown actually has a larger spread in [Mg/Fe] for a given clump compared to the instantaneous case. Finally, when the gas mass is doubled, the gaps between the clumps in the [Mg/Fe]-[Fe/H] plane become less pronounced. This is because, for a fixed iron production rate, the magnitude

How to Find the "Clumps" (Bursts) in the Data

of the [Fe/H] gap is modulated by the underlying gas mass.

3.1. *Quantifying the gap in [Fe/H] between starbursts*

To better understand the impact of bursty star formation on the chemical evolution of dwarf galaxies, we analytically estimate the difference in [Fe/H] between two consecutive starbursts. This difference manifests as the spacing between the peaks of a multimodal MDF in the case of bursty star formation. The spacing between the distinct star formation episodes is determined by the degree to which the metallicity evolves during the quiescent periods separating the starbursts. This evolution is primarily driven by the accumulated reservoir of Type Ia supernovae from previous star formation episodes, which continuously enrich the interstellar medium with iron-peak elements (bottom right panel of Fig 1).

Consider two starbursts separated by a time gap $\delta t_{\rm gap}$. The corresponding gap in [Fe/H] between the first and second starburst, to first approximation, is contributed by the supernovae from the first starburst and can be expressed as

$$\Delta[{\rm Fe/H}] = \log_{10}\frac{M_{\rm Fe}(t)+\Delta M_{\rm Fe}}{M_{\rm Fe}(t)} \approx \frac{\Delta M_{\rm Fe}}{M_{\rm Fe}(t)\ln(10)} \quad (6)$$

where $\Delta M_{\rm Fe}$ is the additional iron mass generated between times t and $t+\delta t_{\rm gap}$. The approximation is a Taylor expansion assuming that the change in total Fe mass during the gap is small compared to the existing Fe mass.

If we assume a starburst generating a total mass M_*, and a power-law delay time distribution given by Equation 2, the gap in [Fe/H] between two starbursts contributed by type Ia supernovae can be approximated as:

$$\Delta[{\rm Fe/H}]_{\rm Ia} \approx \frac{y_{\rm Ia,Fe} r_{\rm Ia} M_*}{\mu_{\rm Fe} M_{\rm g,eff} 10^{[{\rm Fe/H}]-4.5}\ln(10)} \times \int_{t_{\rm min}}^{\delta t_{\rm gap}} 0.429\left(\frac{t}{\rm Myr}\right)^{-1.1} dt \quad (7)$$

where $\log_{10}(N_{\rm Fe}/N_{\rm H})_\odot = -4.5$ so we can express $M_{\rm Fe}(t)$ in terms of [Fe/H]:

$$M_{\rm Fe}(t) = \mu_{\rm Fe} M_{\rm g,eff} 10^{[{\rm Fe/H}]-4.5} \quad (8)$$

Evaluating the integral yields:

$$\Delta[{\rm Fe/H}]_{\rm Ia} \approx \frac{4.29 y_{\rm Ia,Fe} r_{\rm Ia} M_*}{\mu_{\rm Fe} M_{\rm g,eff} 10^{[{\rm Fe/H}]-4.5}\ln(10)} \left[\left(\frac{t_{\rm min}}{\rm Myr}\right)^{-0.1} - \left(\frac{\delta t_{\rm gap}}{\rm Myr}\right)^{-0.1}\right] \quad (9)$$

Furthermore, the Fe contribution from CCSNe is

$$\Delta[{\rm Fe/H}]_{\rm CC} \approx \frac{y_{\rm Ia,CC} r_{\rm CC} M_*}{\mu_{\rm Fe} M_{\rm g,eff} 10^{[{\rm Fe/H}]-4.5}\ln(10)} \quad (10)$$

As the equation shows, the longer the time gap between starbursts, the larger the visible metallicity gap would be, as expected. The gap Δ[Fe/H] is sensitive to the underlying effective mixing gas mass $M_{\rm g,eff}$ and the initial gas metallicity [Fe/H]. The combination of these two effects shows that such gaps should only be more prominent [illegible] of galaxies with lower metallicities and effective gas masses.

To illustrate, consider a gas mass of $M_{\rm g} = 3\times10^6\,{\rm M_\odot}$, a starburst that [illegible] a stellar mass of M_* [illegible] and a burst gap $\delta t_{\rm gap} = 200$ Myr. At the [illegible] licity of [Fe/H] [illegible] we find that the resulting Δ[Fe/H]$_{\rm Ia}$ from Type Ia supernovae in the MDF is approximately 0.15 dex. [illegible] combined with the [illegible] from core-collapse [illegible] to a [illegible] metallicity gap of 0.2 [illegible] which is [illegible] larger than the typical spectroscopic metallicity [illegible]. Even at [Fe/H] = -1.8, if we assume a $\delta t_{\rm gap} = 400$ Myr following the simulations, the expected gap is still about 0.11 dex, which should be measurable in high-resolution spectroscopy. The gap is even more pronounced at lower metallicities, as illustrated in Figure 1 [illegible] the key signal that we aim to detect and quantify in our study.

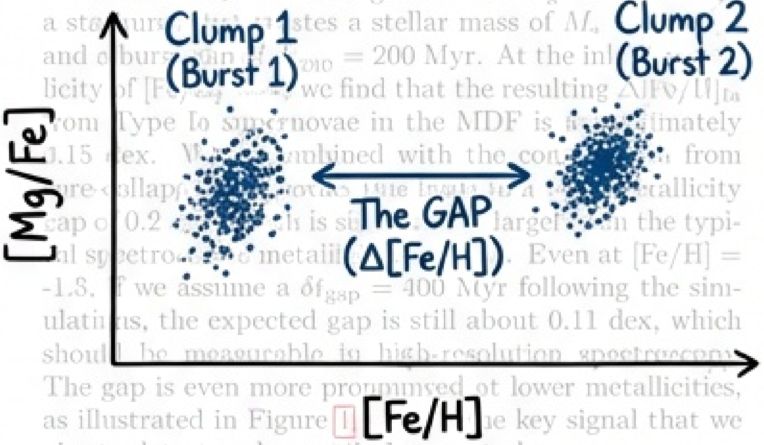

4. MEASURING THE DISCONTINOOUS CHEMICAL TRACK

Our theory developed above suggests that measuring [illegible] by looking for distinct stripes in the [illegible] gaps in the MDF should [illegible] the bursty nature of star formation in these systems. Given [illegible] of our chemical evolution model, we [illegible] the multi-modal [illegible] track in an [illegible] manner [illegible] Gaussian Mixture Models (GMMs) in the [Mg/Fe]-[Fe/H] plane. As the name suggests, GMMs aim to model the chemical space with a mixture of Gaussians, mathematically expressed as:

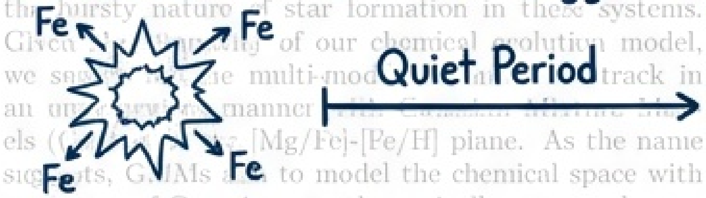

$$p(\mathrm{x}) = \sum_{k=1}^{K} \pi_k \mathcal{N}(\mathrm{x}|\mu_k, \Sigma_k) \quad (11)$$

where x = ([Fe/H], [Mg/Fe]) represents a data point in the chemical space, K is the number of Gaussian components, [illegible] mixing coefficients [illegible] of the k-th component [illegible] $\sum \pi_k = 1$, and [illegible] denotes the [illegible] Gaussian density with mean μ_k and covariance matrix Σ_k.

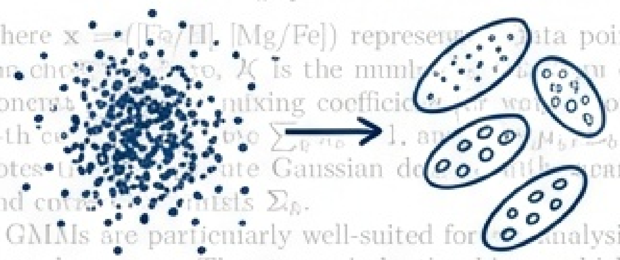

GMMs are particularly well-suited for [illegible] analysis for several reasons. The strong inductive bias - which assumes the data can be modeled [illegible] of Gaussian components - allows us to perform robust modeling with our small dataset (~100 stars). [illegible] tion is certainly a limitation, in the absence of measurement uncertainties, chemical evo[illegible] defined one-dimensional paths, with observed spread primarily reflecting measurement uncertainties. And chemical abundance uncertainties are approximately Gaussian [illegible] features. We find that while more flexible density estimation methods exist (e.g., Normalizing Flows Ting and We[illegible] components - exactly what we expect from episodic star

Putting our 'Un-mixing' Tool (GMMs) to the Test!

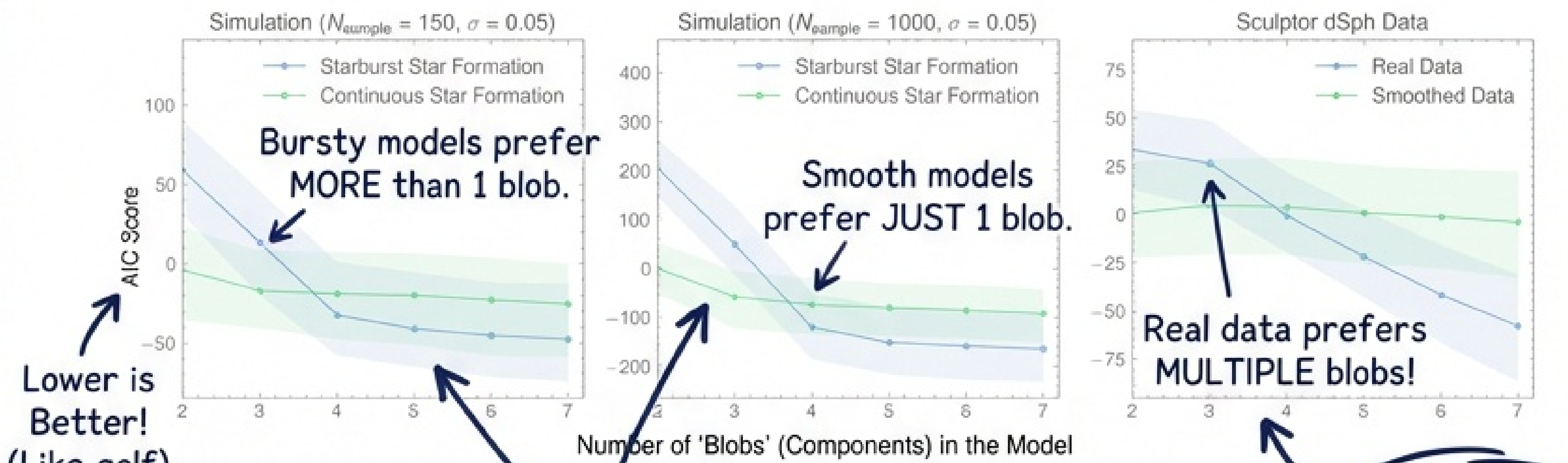

Figure 2. Detecting discontinuous sta formatn by searching for nultimodal components in the chemical tracks ... Models. The figure shows the Alaike Iulornation Criterion score versus the number of components assumed in the ... indicating that the model is favored. The sh...l region shows the 1σ uncertainty from bootetropping. In the bursty ... if the measurement precision is comparsbin to so smaller than the gap hetween the dicontimious chemical tseas, w... would be preferred. The left and m... d in Figure 1, whi... the case of real APOGEE data for the ... The figure tatzontrates that, even fo a lin... 150 and limited precision in the abundanc... signal in the AIC score de... estimate the AIC score for the simulatione using 100 realizations and bootstrapping for the real data to estimate the ...rtainty. A larger sample of 1000 stars, as shown in the middle panel, will lead to an unambiguous detection of multimodality. In the case of the real data, which more closely aligns with the simulated case in the left panel, we demonstrate statistical evidence for multimodality in the Sculptor dwarf spheroidal galaxy; the AIC score is higher for a larger number of components, superseding the sampling noise, suggestive of bursty star formation. The real data also shows a more prominent signal at larger number of components, presumably due to the fact that, unlike assumed in the simulations, the gas mass varies as a function of time, leading to individual Gaussian modes being more distinct than in the simulations.

So, the tool works on fake data! It can tell the difference.

EVIDENCE for BURSTS in a REAL Galaxy!

formation. As we will see, to ensure robust results despite these limitations, we carefully validate our GMM fits through bootstrap resampling and comparison with smoothed models (see Figure 2) with simulated data, finding the method is adequate to find statistical evidence for multimodality in our dataset.

To determine the best-fitting model, we fit GMMs with different numbers of components to the chemical space and compare their likelihoods, defined as:

$$L(\theta) = \prod_{i=1}^{N} p(x_i|\theta) \quad (12)$$

where $\theta = \{\pi_k, \mu_k, \Sigma_k\}_{k=1}^{K}$ represents the set of all parameters in the GMM, and N is the number of data points.

Finding the optimal parameters for a GMM is a complex non-convex optimization problem that cannot be solved analytically. We therefore fit GMMs using the Expectation-Maximization (EM) algorithm implemented in scikit-learn, which iteratively estimates the model parameters by alternating between two steps: (1) computing the probability of each data point belonging to each component (E-step), and (2) updating the model parameters to maximize the likelihood given these probabilities (M-step). The EM algorithm is guaranteed to converge to a local optimum, but may not find the global optimum. To address this limitation, we perform 1000 independent fits with different random initializations, validating that each component has at least 4 points and covariance correlations below 0.9, and select the model with the highest likelihood score. This approach helps avoid poor local optima and ensures robust convergence to a well-behaved solution that accurately captures the underlying structure in the data.

It is important to note that GMMs with more components will have a strictly better likelihood than their lower-component counterparts: setting the weight of an additional component to zero to ... case. To properly evaluate the ... need to penalize models bas... this study, we use the Akaike Information Criterion ... Akaike 1974) defined as:

AIC is like a referee trying to find a balance.

Good Fit — Complexity

$$\mathrm{AIC} = 2m - 2\ln(\hat{L}) \quad (13)$$

where m is the number of parameters in the GMM ($K(1 + d + (d(d+1))/2) - 1$ for a 2-dimensional GMM, where K is the number of modes and $d = 2$ the dimension), and $\hat{L}$ is the maximum likelihood estimate of the model. A lower AIC is better.

It rewards a model that fits well, but penalizes it for being too complicated (too many blobs).

Based on the AIC score, we ... number of Gaussian component... data. The AIC balances model ... plexity according to the equati... indicates a more favorable trade... and fit. Specifically, $-2\ln(\hat{L})$ rewards models that better fit the data, while $2m$ penalizes complex models. Under the assumption that the true model lies within the family of candidate models, AIC is asymptotically optimal in selecting the model closest (in a Kullback–Leibler sense) to the true process (Akaike 1974). When the preferred model includes multiple Gaussian components, this naturally suggests multimodality in the chemical abundance space

If the best AIC score is for MORE than 1 component, it means those "blobs" (and therefore the bursts) are likely REAL!

The Moment of Truth: Applying our tool to a REAL Galaxy (Sculptor)!

physical context, such a pattern is consistent with bursty star formation, wherein different episodes of star formation give rise to distinct chemical loci.

To demonstrate the effectiveness of GMMs in detecting discontinuous chemical tracks, we start with a mock sample as depicted in Figure 1. We consider two scenarios: the fiducial model with regular starbursts spaced between 150-450 Myr apart (the blue SFH in the top right panel of Figure 1) with each starburst lasting 150 Myr; and the continuous smooth star formation model that integrates to the same total stellar mass of $10^7 M_\odot$ (the dashed orange line in Figure 1). We draw samples according to the respective star formation rates and assume an uncertainty of 0.05 dex in both [Fe/H] and [Mg/Fe], similar to the quoted precision and intrinsic dispersion of APOGEE abundances in Sculptor (Mead et al. 2024).

The results are presented in the left and middle panels of Figure 2. The left panel shows a realistic case of current observations, a sample size of 150 stars with Mg and Fe measurements (Kirby et al. 2011a, Hill et al. 2019 (Abdurrouf et al. 2022). The figure demonstrates that even with current observations, the case drawn from bursty star formation favors is able to resolve at least 4 components, as evident from the continuously decreasing AIC scores with a higher number of components. In contrast, the continuous star formation case exhibits nearly flat AIC scores with respect to the number of components, demonstrating that AIC is a reasonable penalty. However, the shaded bootstrap uncertainties in the AIC values indicate that sampling uncertainty cannot be neglected with only 150 stars.

This situation improves if we can further extend the sample size to 1000 stars, as shown in the middle panel. In this case, the sampling noise on the AIC scores decrease substantially and improve the ability to detect multimodality. Obtaining abundances of over 1000 stars in massive dSphs like Sagittarius, Fornax, and Sculptor will soon be possible with spectroscopic surveys on 4-5m telescopes like 4DWARFS (Skuladorn et al. 2023) and Subaru PFS (Takada et al. 2023). The advent of ELTs will enable such measurements in all but the faintest dSph galaxies (Ji et al. 2019). Although not shown, our tests indicate that measurement precision is less critical than sample size for detecting multimodality in these systems. The metallicity gaps, particularly at low [Fe/H], are typically h… ypical spectroscopic unce… metallicities ([Fe/H] $\gtrsim$ … gaps ($\sim$100 higher … help better the mul… m [6].

We need LOTS of stars to see these clumps clearly. Future big telescopes (like ELTs & Subaru PFS) will be game-changers for this!

DETECTING BURSTY STAR FORMATION IN THE SCULPTOR DSPH

We now focus on real observations of the Sculptor (Scl) dSph. The Sculptor dSph is $\approx$84 kpc away (Martinez-Vázquez et al. 2015), with a dynamical mass $\sim 10^8 M_\odot$ (Breddels et al. 2012; Salvadori et al. 2008) and a present stellar mass of roughly $\sim 3-8\times10^6 M_\odot$ (Salvadori et al.

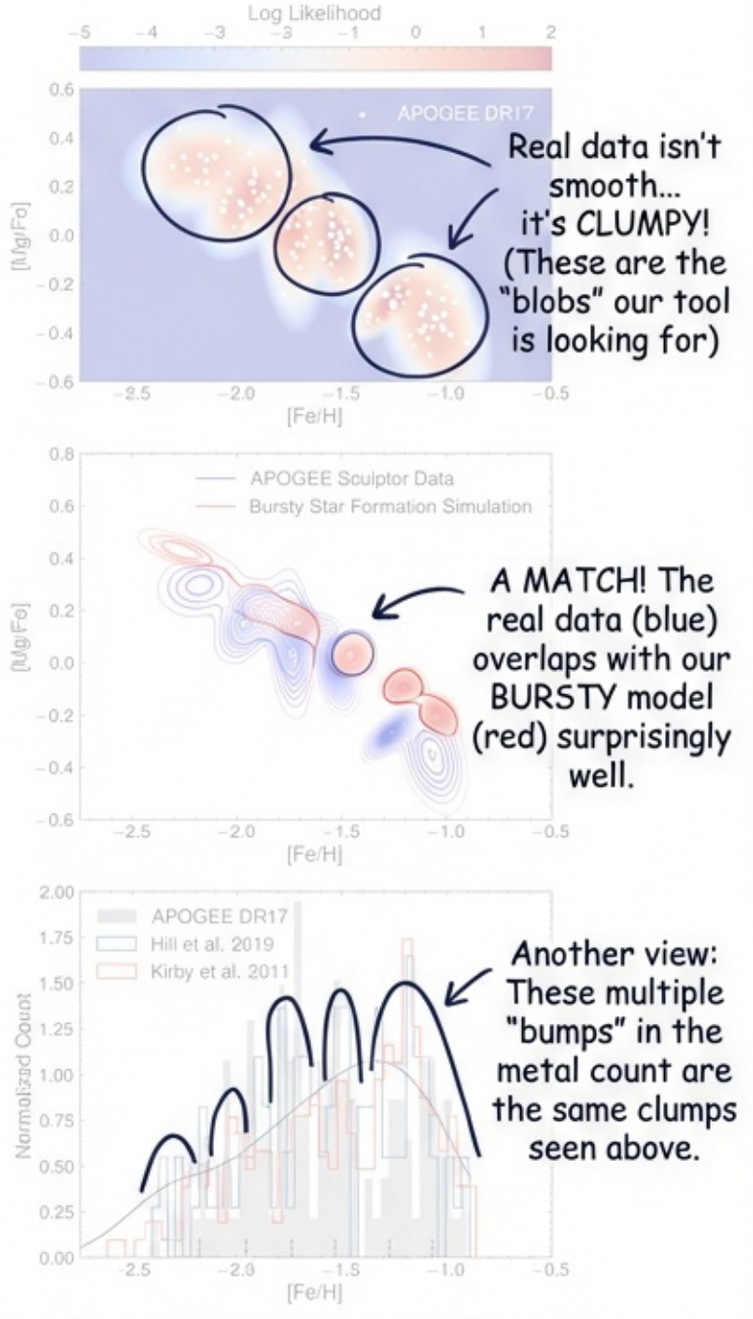

Figure 3. The APOGEE Sculptor dwarf spheroidal galaxy data shows multimodality in the [Mg/Fe]-[Fe/H] plane and metallicity distribution function. The top panel displays the APOGEE Sculptor sample, with the background representing the likelihood from the best-fit 6-component Gaussian Mixture Model. The middle panel compares the likelihood contours of the observed data (blue) with a 6-component GMM fit (red) to an equal number of samples drawn from our simulated bursty star formation model. The similarity between the contours of the observed data and the simulated model reinforces the interpretation of episodic star formation in Sculptor. The bottom panel presents the histogram of [Fe/H] for the APOGEE sample, also exhibiting multimodality. The multimodal distribution aligns well with other Sculptor samples from Hill et al. (2016) and Kirby et al. (2013). The vertical lines in the bottom panel indicate the fitted means of the GMM components, and the solid black line shows the smoothed MDF of the simulated sample.

We used real chemical data from the APOGEE survey for stars in the Sculptor dwarf galaxy...

...and carefully selected stars that are definitely members of Sculptor (based on how they move) to avoid contamination.

The text here is analyzing the plots we just saw on the previous page. The chemical "bumps" in the real data are our real and match our "bursty" model!

We checked our results against other independent studies, and they agree! This gives us confidence in our findings.

Our AIC "referee" (from a few pages back) confirms:

a model with multiple bursts fits the real Sculptor data much better than a smoothe, continuous one.

Interesting detail: The real data is even "burstier" than our simulation! We think this is because real galaxies have varying amounts of gas, while our simple model assumed it was constant.

TIME TO WRAP UP & DISCUSS!

Summary of our main contribution:

We built a theory showing how bursty star formation leaves a unique 'fingerprint' in a galaxy's chemistry.

Let's zoom in on the details of this 'fingerprint'...

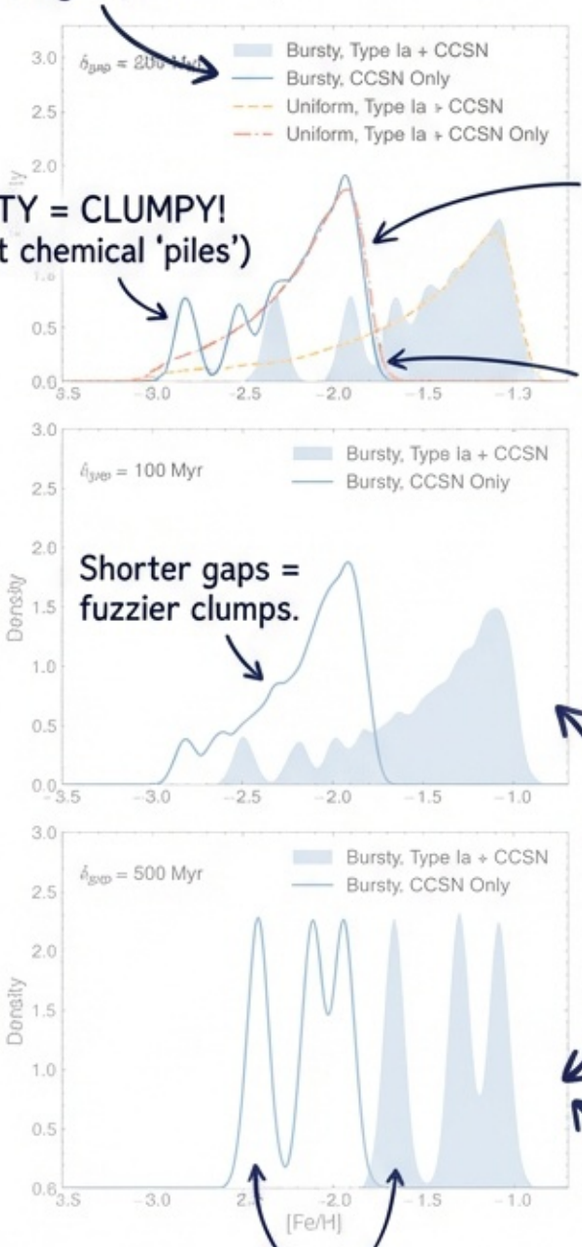

The **TIME** between bursts matters!

More time allows the 'slow' iron factory (Type Ia SNe) to work during quiet periods, work during quiet periods, creating bigger chemical gaps between the bursts.

Chemical Method

Other Methods

Our chemical method acts like a high-resolution camera, seeing short, sharp bursts (~100 Myr) that other techniques miss!

This links our local dwarf galaxy work to what JWST is seeing in the distant, early universe!

Basically, the chemistry records the history of star formation like tree rings... but with **EXPLOSIONS**!

Figure 4. The contribution from Type Ia supernovae enhances the prominence of multimodality in the metallicity distribution function. The figure presents star formation histories, each integrating over 2 Gyr and assuming a mixing gas mass of $3 \times 10^8 M_\odot$. The shaded blue region in the top panel depicts the MDF for the fiducial case with instantaneous bursty star formation and a gap (δt_{gap}) of 200 Myr. For comparison, the top panel also includes the MDF for uniform and continuous star formation, represented by the dot-dashed red and dashed orange lines. In these cases, the MDF is smooth and lacks multimodality.

ous star formation. In particular, we expect to find multiple modes in the [Mg/Fe]-[Fe/H] plane and in the metallicity distribution function. We adopt Gaussian Mixture Models to detect such multimodality, as they are model-agnostic. As a proof of concept, we apply this method to the existing APOGEE data of the Sculptor Sph galaxy.

We find that the AIC score trend is distinguishable from the smoothed case. The observed signatures are consistent with other datasets of Sculptor as well as the theory developed, supporting an episodic star formation history galaxy.

Time Resolution for Dwarf Galaxy Star Formation Histories

In Figure 4, we emphasize that the strength of the multimodal signal relies on the production of Fe by Type Ia ashed ow the ormly over ashed orange line in the top-left corner of Figure $I_\odot$. In this case, with or without Type Ia supernovae, the MDF is smoothe shaded blue region shows the expected MDF from the starburst case, where we assume instantaneous starbursts of $10^6 M_\odot$, spanning 2 Gyr with a starburst gap of 200 Myr (i.e., the black line in Figure $I_\odot$). In this case, the multimodality is clearly seen at [Fe/H] $\lesssim -1.5$, though it is harder to detect at higher metallicities. If we then remove Type Ia supernovae, as shown by the solid blue line, the gap is more subdue becomes invisible after [Fe/H] > -2.5. We show a and longer in the other two panels, illustrat multimodality can be resolved even down

Such high time resolution in ar formation histories of local d 2012] which impose smooth star formation histories that preclude bursty or episodic star formation (e.g., Vincenzo et al [2023] Weinberg et al [2017, de los Reyes et al [2024, Sandford et al [2024].

The episodic star formation we suggest occurs in Sculptor may be consistent with recent JWST observat of high redshift galaxies that display minlquench (Antwi-Danso 2024] Dome et al [2024, Looser et al [2 but for galaxies whose steller mass is much l could be detected directly at high redshift. The progenitor of Sculptor has M et al [2024], which is the lowest mass spectr $z \sim 7$ (Atek et al [2024 provide imprecedented time resolution for the star formation histories of early low mass galaxies.

A natural question is whether even shorter timescales of ~10 Myr could be resolved by chemical evolution. Indeed we assumed that all CCSN produce Mg at a single time, but in reality there is a delay time distribution for CCSNe as well lasting from 3-30 Myr (e.g., de los Reyes et al [2022). We found this is unlikely to be for moss galaxies, as repeated bursts on signature from a al [2

2022) may still exhibit these signatures.

6.2. *Intrinsic spread in [α/Fe] from the starbursts*

Initially, we had anticipated that the [Mg/Fe] spread would be an independent useful indicator of bursty star formation. This was motivated by past studies (e.g. [Reochi and Kroupa 2013, Muley et al [2021, Patel et al [2021, Mead et al. 2021) and by the sharp sawrooth [Mg/Fe] vs [Fe/H] pattern in Figure 1. However, detecting and using the [Mg/Fe] spread turns out to be substantially more difficult than the [Fe/H] gaps in the model presented here. Observationally, this is because it is much harder to detect an intrinsic scatter than a difference in means: the uncertainty on intrinsic scatter seples as $N_*^{1/4}$ while means scales as $N_*^{1/2}$ (see Ting and Weinberg 2022). Theoretically, it is because star formation bursts have to be somewhat fine-tuned to capture the maxinum [Mg/Fe] spread: a burst must be longer than 10 Myr to capture any Mg being produced, and shorter than 100 Myr so Type Ia supernovae do not start contributing to Fe. Even when this happens, the sigual is quite small.

Following Section 3, we can approximate the expected spread in [Mg/Fe] with:

$$\Delta[\mathrm{Mg/Fe}] \approx \frac{y_{\mathrm{CC},M_\odot} r_{\mathrm{CC}} M_*}{\mu_{\mathrm{Mg}} M_{\mathrm{g,eff}} 10^{[\mathrm{Mg/H}]-4.4} \ln(10)} - \frac{y_{\mathrm{CC},\mathrm{Fe}} r_{\mathrm{CC}} M_*}{\mu_{\mathrm{Fe}} M_{\mathrm{g,eff}} 10^{[\mathrm{Fe/H}]-4.5} \ln(10)} \quad (14)$$

where we have neglected the SNIa contribution assuming that it is small in the burst.[2] Assuming [Mg/Fe] = 0.4, an integrated star formation of $M_* = 10^6\,\mathrm{M}_\odot$, and a gas mass of $M_{\mathrm{g,eff}} = 3 \times 10^9\,\mathrm{M}_\odot$, we estimate that Δ[Mg/Fe] changes by only 0.08 dex at [Fe/H] = -2, decreasing to 0.02 dex at [Fe/H] = -1.5. However, our assumption of instantaneous mixing into a large constant effective gas mass for CCSN may hinder our ability to resolve this signal, and concentrating the Mg into a smaller gas mass would enhance the signal (e.g., Emerick et al. 2018, Patel et al. 2022).

6.3. *Quantitative Interpretation of the [Fe/H] Gaps in Sculptor*

In Section 5 and the bottom panel of Figure 3, we see that the spacing between adjacent bursts veries from 0.20 to 0.25 dex, with larger separations occurring at lower metallicities, which is quite uniform. From Equation 9, assuming Type Ia supernovae contribution dominates the gap, this implies that the quantity $(M_*/M_{\mathrm{g,eff}})[(t_{\mathrm{min}}^{-0.1} - t_{\mathrm{gap}}^{-0.1})/10^{[\mathrm{Fe/H}]}]$ remains approximately constant throughout the galaxy's evolution. In our model, we have assumed $(M_*/M_{\mathrm{g,eff}})$ is constant, and adjusted t_{gap}, to match this observed spacing. As shown in the middle panel of Figure 3, we find that a gradual increase of δt_{gap} from 150 Myr to 450 Myr with an increment of 30 Myr per starburst (see the top right panel of Figure 5) leads to a good qualitative match to the data (see the middle panel of Figure 5). It was not required that the burst separations fit into the 2 Gyr duration of Sculptor's formation history, but it does, suggesting that taking $M_{\mathrm{g,eff}}$ to be constant is a reasonable approximation.

Furthermore, we can try to interpret the intrinsic scatter in [Mg/Fe]. We estimate the intrinsic scatter of each component from our GMM fit, taking the fitted covariance matrices Σ_k and subtracting 0.05 dex in quadrature as a typical uncertainty. The measured scatters for the three prominent modes at [Fe/H] $\simeq$ -1.74, -1.53, and -1.27 are found to decrease from 0.13, 0.08, to 0.05 dex, respectively. Following Equation 14, if we take $M_{\mathrm{g,eff}}$ to be consi… follows the ratio… letely explained… gas mass (also … clusion on r-process scatter in …

These calculations are clearly primitive, and a full interpretation should more carefully consider evolution of $M_{\mathrm{g,eff}}$. However, the fact that we could find a suitable bursty st… the observ… licity dis… lution wi… should not vary…

6.4. *Starburst Signals from Other Dwarf Galaxies*

While we chose to study the Sculptor dSph galaxy in this work due to the availability of multiple datasets that corroborate our results and its status as one of the most well-studied dwarf galaxies, other galaxies could potentially show evidence for bursty star formation.

To demonstrate the expected signal, in Figure 5, we show the expected metallicity gap as a function of the time gap in star formation, δt_{gap}, as well as the metallicity of the galaxy, following the theory developed in Section 3.1). The solid white lines in the figure represent Δ[Fe/H] values of 0.05 dex, 0.1 dex, and 0.3 dex, which signify the typical uncertainty of metallicity from high-resolution ($R \simeq 20,000$), mid-resolution ($R \simeq 6,000$) … vely. … the … predi… the ratio … integra… mass, … here, … history … that k… mass o… $10^8\,\mathrm{M}_\odot$, i.e., a ratio of 1/30.

Very few dwarf galaxies have enough metallicities to directly measure a multimodal MDF on the 100s of Myr timescales that we propose for Sculptor. However, many galaxies have clear stagnant periods lasting >1 Gyr that are clearly distingnished using main sequence

[2] The exponent for [Mg/H] has the term -4.4 instead of -4.5 (as seen in [Fe/H]) dne to a slight difference in the solar normafisation values for nugnesium and iron. According to Asplund et al. (2009), there's a 0.1 discrepancy between these clements.

[3] To be more exact, we choose not to use the Taylor expansion (Espution 5,, but rather perform the full numerical evaluation for this caiculation.

We *thought* [Mg/Fe] (alpha-elements) would be a good indicator, but the signal is too small and gets "washed" out" easily. Iron ([Fe/H]) is better!

QUANTIFYING THE GAPS: The *size* of the chemical gaps tells us the *time* between bursts!

Crucial Detail: To match the real Sculptor data, the time *between* bursts had to INCREASE over time (from ~150 to ~450 Myr).

BROADENING THE SEARCH: Now we look for these "starburst signals" in *other* dwarf galaxies.

Figure 5 (next page!) will show us what to look for.

OK, let's check our "starburst signal" against OTHER dwarf galaxies...

☑ WLM & Carina: Predicted chemical gaps generally match observations! (Score!)

? Reticulum II: A bit of a puzzle. Might need to adjust our model (e.g., gas loading factors).

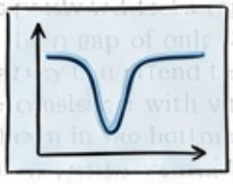

PREVIEW OF FIGURE 5 (It's coming!): This figure will show us the predicted 'fingerprint' of these gaps in the chemical data. Keep an eye out for the 'dips'!

CAVEATS & LIMITATIONS

(Honesty is the best policy in science!)

1. The SN Ia "Clock" is Slow: Our method's time resolution is limited by the delay time of Type Ia supernovae. We can't see super-short bursts.

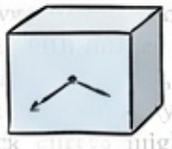

MODEL REALITY

2. The 'Constant Gas' Assumption Again: Remember that 'effective mixing gas mass' ($M_{g,eff}$)? Assuming it's constant is a BIG simplification. Real galaxy plumbing is messier.

Putting our model to the test with real data!

Galaxy	$\delta t_{\rm gap}$ (Gyr)	[Fe/H]	Observed [Fe/H] Gap	Predicted [Fe/H] Gap*	References
Sculptor	0.3 ± 0.15	-1.9 ± 0.6	$0.20 - 0.26$	0.20	This Work
WLM	3 ± 1	-1.7 ± 0.3	0.3	0.26	1
Carina	4.5 ± 2.5	-1.8 ± 0.3	0.35	0.36	2,3
Reticulum II	3.4 ± 1	-2.6 ± 0.1	0.04	1.09 (0.65*)	4,5

Pretty good match!

Comparing what we see vs. what our toy model predicts.

Missed this one. Needs a better "plumbing" model (as noted before).

Table 1

Comparison of star formation quiescent periods ($\delta t_{\rm gap}$) and [Fe/H] gap between star formation episodes, the metallicity distributions. For each galaxy, the observed metallicity

References. 1: McQuinn et al. 2024 2: Norris et al. 2017a 3: Norris et al. 2017b 4: Simon et al. 2023 5: Ji et al. 2023 and Luna et al. in prep.

*: The predicted [Fe/H] gap is based on a stellar mass to mixing gas mass ratio of 1/30. The value in brackets shows the prediction if we assume a ratio of 1/70 instead.

Here's the "fingerprint" plot we previewed!

The "Chemical Gap Map".

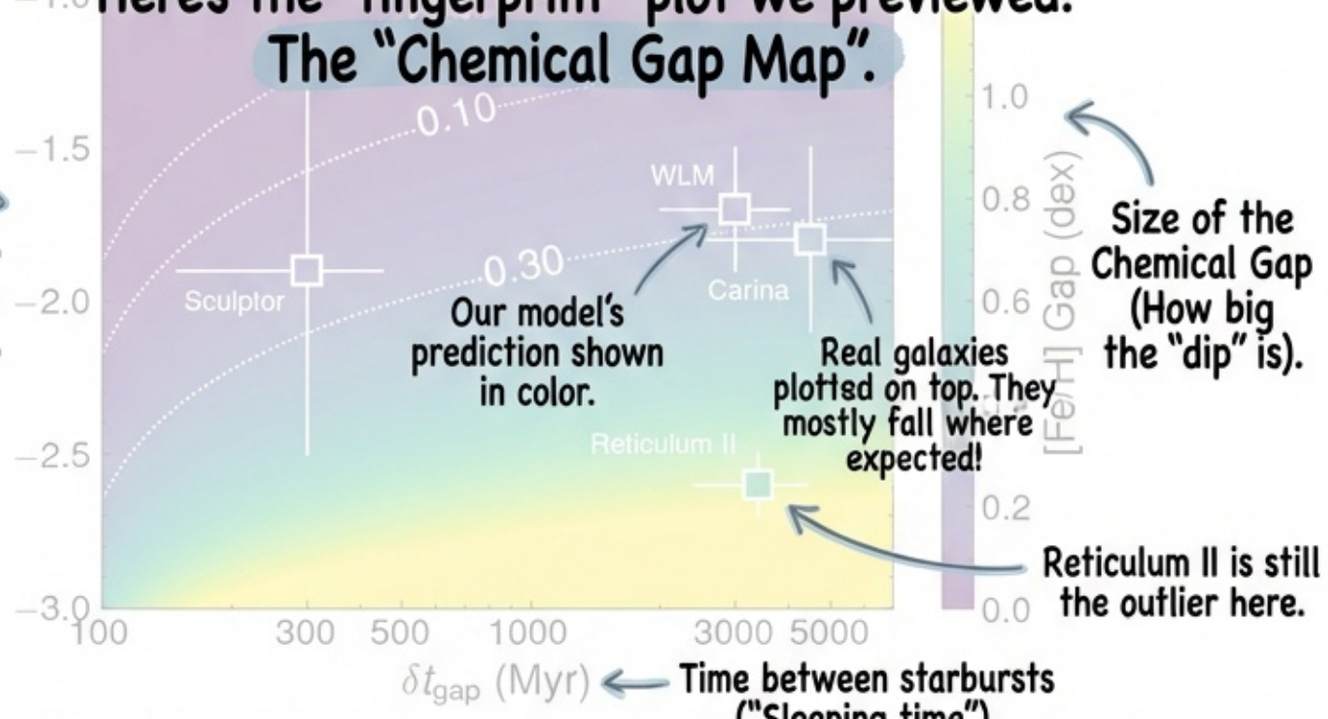

Initial Metal Content ("Starting ingredients").

Our model's prediction shown in color.

Real galaxies plotted on top. They mostly fall where expected!

Size of the Chemical Gap (How big the "dip" is).

Reticulum II is still the outlier here.

Time between starbursts ("Sleeping time").

Figure 5. The predicted metallicity gap in the metallicity distribution function as a function of the characteristic metallicity and starburst time gap. The white dotted lines include the typical uncertainties of metallicity measurements from high-resolution spectroscopy ($R \simeq 20,000$, 0.05 dex), mid-resolution spectroscopy ($R \simeq 6,000$, 0.1 dex), and photometric metallicities (0.3 dex). Overplotted are measurements from a few dwarf galaxies. The Sculptor dwarf galaxy data points are measured in this study by matching the [Mg/Fe]-[Fe/H] contours. For the other galaxies, Carina, WLM and Reticulum II, the starburst time gap is estimated from color-magnitude diagrams, and the metallicity gap (represented by the color of the symbols) is determined from the [Fe/H] distribution. Despite the simplicity of our analytic model, it accurately predicts the metallicity gaps when assuming an integrated SFR to mixing gas mass ratio of 1/30.

star formation. Future work incorporating time-varying gas masses will help quantify how feedback efficiency impacts the visibility and interpretation of these chemical signatures across different mass scales (e.g., Agertz et al. 2013; Read et al. 2016).

7. CONCLUSION

In this initial foray into the impact of episodic star formation on chemical evolution, we develop a model to describe bursty star formation and its impact on the chemical properties of stars. We have demonstrated that episodic star formation in dwarf galaxies leads to distinct chemical signatures compared to continuous star formation scenarios. The multimodal chemical signature provides access to timescales much shorter than possible

THE BIG PICTURE WRAP-UP.

1. Bursty star formation creates clear 'chemical gaps' & 'clumps'.

2. These signals are created by the delay of Type Ia Supernovae.

3. The good news: These features are BIG enough to see with telescopes we have right now!

already detectable, with sufficient statistical significance according to the Akaike Information Criterion, in current datasets of $\mathcal{O}(100)$ stars. However, larger samples remain important for reducing sampling noise and improving the robustness of the results.

As a proof of concept, we apply our model to the APOGEE data of the Sculptor dSph galaxy. Our findings are:

- Using Gaussian Mixture Models and the Akaike Information Criterion, we show that the [Mg/Fe]-[Fe/
- We
- Bas
- We

to other dwarf galaxies with Gyr-long quiescent periods that could be probed with color-magnitude diagrams, including WLM, Carina, and Reticulum II.

THE FINAL VERDICT ON SCULPTOR:

- ☑ 1. Stats & Sims confirm: Star formation was BURSTY, not smooth!
- ☑ 2. Sculptor took 'naps' (quiescent periods) lasting ~150-450 Million Years.
- ☑ 3. Matches what JWST sees in other galaxies ('miniquenching') & extends it to fainter ones!

While our theory and analysis are admittedly simplistic, this study paves the way for a more comprehensive understanding of the complex interplay between episodic star formation, feedback, and the mixing gas mass in dwarf galaxies. Crucially, our work provides a theoreti-

WHY THIS MATTERS FOR THE FUTURE:

Current models are too 'smooth'.

We need 'bursty' models to interpret data from upcoming BIG telescopes.

Our simple theory is a foundation for that!

these and other models that take full advantage of the recent and upcoming major advances in chemical abundance quality and quantity.

We gratefully thank the Research School of Astronomy and Astrophysics at the Australian National University for supporting A.P.J.'s visit as part of the Distinguished Visitor Program, during which this work was initiated. We also appreciate the serene environment of Canberra, the company of marsupials, and the abundant rabbit population on the ANU campus. The environment provided an ideal setting for in-depth discussions about this project. The inspiration for this study arose from a conversation with An[illegible]during Y.S.T.'s recent vi[illegible] Pratik Gandhi, Erwi[illegible] Limberg, Evan Kirby, [illegible] Kratsov, a[illegible] over the y[illegible] Y.S.T. ARC DEC[illegible]rch [illegible] supporte[illegible] National Science Foundation grants AST-22[illegible]nd AST-2307599.

Science happens in interesting places! Shout out to the marsupials & rabbits at ANU in Canberra for the 'serene environment'.

REFERENCES

F. Governato, C. Brook, L. Mayer, A. Brooks, G. Rhee, J. Wadsley, P. Jonsson, B. Willman, G. Stinson, T. Quinn, et al., Nature **463**, 203 (2010), 0011.2237.
P. F. Hopkins, D. Kereš, J. O norbe, C.-A. Faucher-Gigu'ere, E. Quataert, N. Murray, and J. S. Bullock, MNRAS **448**, 3S1 (2014), 1311.2023.
T. K. Chan, D. Kereš, J. O norbe, P. F. Hopkins, A. L. Muratov, C. A. Faucher-Gigu'ere, and E. Quataert, MNRAS **484**, 2951 (2013), 1507.02282.
A. A. Dutton, A. V. Macciò, A. Dekel, L. Wang, G. Stinson, A. Obreja, A. Di Cintio, C. Brook, T. Buck, and X. Kang, MNRAS **461**, 2658 (2016), 1605.05323.
E. Tollet, A. V. Macci'o, A. A. Dutton, G. S. Stinson, L. Wang, C. Penso, T. A. Gutcke, T. Buck, X. Kang, C. Brook, et al., MNRAS **456**, 3542 (2016), 1507.03590.
S. Bose, C. S. Frenk, A. Jenkins, A. Fattahi, F. A. G'omez, R. J. J. Grand, F. Marinacci, J. F. Navarro, K. A. Oman, R. Pakmor, et al., MNRAS **486**, 4790 (2019), 1810.03035.
N. Emami, B. Siana, D. R. Weisz, B. D. Johnson, X. Ma, and K. El-Badry, ApJ **881**, 71 (2019), 1608.06380.
J. Bland-Hawthorn, R. Sutherland, and D. Webster, ApJ **807**, 154 (2015), 1303.00209.
C. Wheeler, P. F. Hopkins, A. B. Pace, S. Garrison-Kimmel, M. Boylan-Kolchin, A. Wetzel, J. S. Bullock, D. Kereš, C.-A. Faucher-Gigu'ere, and E. Quataert, MNRAS **490**, 4447 (2019), 1812.02710.
Y. Hirai, E. N. Kirby, M. Chiba, K. Hayashi, R. Anguiano, T. R. Saitoh, M. N. Ishigaki, and T. C. Beers, arXiv preprint arXiv:2405.05330 (2024).
C. Galiart, M. Monelli, T. Rnie-Lara, A. Caiamida, S. Cassisi, M. Cignoni, J. Anderson, G. Battaglin, J. R. Dermojo-Climent, E. J. Bernard, et al., ApJ **908**, 102 (2021), 2101.04464.
L.-H. Chen, M. Maag, T. Hartwig, S. C. O. Glover, A. P. Ji, and R. S. Klessen, MNRAS **513**, 934 (2022), 2202.01220.
A. Savino, D. R. Weisz, E. D. Skillman, A. Dolphin, A. A. Cole, N. Kallivayalil, A. Wetzel, J. Anderson, G. Beala, M. Boylan-Kolchin, et al., ApJ **956**, 86 (2023), 2305.13360.
K. B. W. McQuinn, Y.-Y. Mao, M. B. Buckley, D. Shih, R. E. Cohen, and A. E. Dolphin, ApJ **944**, 14 (2023), 2301.04157.
K. B. W. McQuinn, M. J. B. Newman, A. Savino, A. E. Dolphin, D. R. Weisz, B. F. Williams, M. L. Boyer, R. E. Cohen, M. Correnti, A. A. Cole, et al., ApJ **961**, 16 (2024), 2312.03060.
J. F. Navarro, C. S. Frenk, and S. D. M. White, Ap[illegible] (1996), astro-ph/9509025.
A. Pontzen and F. Governato, [illegible] 1106.0388.
G. San[illegible] MN[illegible]
L. Clo[illegible] Bea[illegible] e-pri[illegible]
J. B. M[illegible] C. M[illegible] prints arXiv:2404.07250 (2024), 2404.07250.

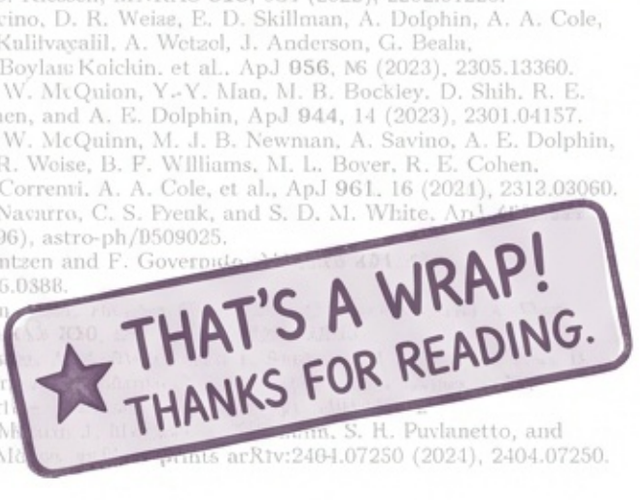


THE FOUNDATION OF IT ALL:
STANDING ON THE SHOULDERS OF GIANTS!
A PhD is basically just reading a *lot* of papers... and then adding one more to the pile. Thanks to everyone who came before me!
REFERENCES
PAST RESEARCH
SCIENCE IS A TEAM SPORT!

And the list goes on... and on...
It really highlights how every new paper is just one small brick in a massive wall of knowledge built by thousands of others. Truly humbling.

J. D. Simon, T. M. Brown, B. Mutlu-Pakdil, A. P. Ji, A. Dvlica-Wagner, R. J. Avila, C. E. Martínez-Vázquez, T. S. Li, E. Balbinot, K. Bechtol, et al., ApJ **944**, 43 (2023), 2212.00810.
R. Leamon, K. A. Venn, A. M. Brooks, G. Battaglia, A. A. Cole, R. A. Ibata, M. J. Irwin, A. W. McConnachie, J. T. Mendel, E. Starkenburg, et al., ApJ **767**, 131 (2013), 1302.1879.
J. E. Norris, D. Youg, K. A. Venn, G. Gilmore, L. Casagrande, and A. Dotter, ApJS **230**, 28 (2017b), 1705.00023.
A. P. Ji, J. D. Simon, I. U. Roederer, E. Magg, A. Frebel, C. I. Johnson, R. S. Klessen, M. Magg, G. Cescutti, M. Mateo, et al., AJ **165**, 100 (2023), 2207.03499.
R. K. Alexander, F. Vincenzo, A. P. Ji, H. Richstein, C. J. Jordan, and B. K. Gibson, MNRAS **523**, 5413 (2023), 2303.12580.
H. Jönsson, J. A. Holtzman, C. Allende Prieto, K. Cunha, D. A. García-Hernández, S. Hasselquist, T. Masseron, Y. Osorio, M. Shetrone, V. Smith, et al., AJ **160**, 120 (2020), 2007.05337.
S. E. Koposov, C. A. Prieto, A. P. Cooper, T. S. Li, L. D. e Silva, B. Kim, A. Carcillo, A. Dey, C. J. Manser, F. Nikakhtar, et al., MNRAS (2024), 2407.06280.
O. Agertz, A. V. Kravtsov, S. N. Leitner, and N. Y. Gnedin, ApJ **770**, 25 (2013), 1210.4957.
J. I. Read, O. Agertz, and M. L. M. Collins, Monthly Notices of the Royal Astronomical Society **458**, 2573 (2016), ISSN 0035-8711, https://academic.oup.com/mnras/article-pdf/458/3/2573/6105757/stw713.pdf, URL http://doi.org/10.1093/mnras/stw715

Huge respect for **Open Science** initiatives! 🔓 Publishing in open-access journals means anyone, anywhere can read this research for free. That's how science **should** be! 🌍✨

This paper was built using the Open Journal of Astrophysics LaTeX template. The OJA is a journal which provides fast and easy peer review for new papers in the astro-ph section of the arXiv, making the reviewing process simpler for authors and referees alike. Learn more at http://astro.theoj.org

Alright, that's a wrap! Thanks for joining me on this deep dive into the messy, bursty lives of dwarf galaxies. It's been fun! Now, time for a nap... 😴